High resolution Shack-Hartmann sensor based on array of nanostructured GRIN lenses

Research Article | Vol. 25, No. 3 | 6 Feb 2017 | OPTICS EXPRESS 1680

Optics EXPRESS

High resolution Shack-Hartmann sensor based on array of nanostructured GRIN lenses

RAFAL KASZTELANIC,[1,*] ADAM FILIPKOWSKI,[1] DARIUSZ PYSZ,[1] RYSZARD STEPIEN,[1] ANDREW J. WADDIE,[2] MOHAMMAD R. TAGHIZADEH,[2] AND RYSZARD BUCZYNSKI[1,2,3]

[1]*Institute of Electronic Materials Technology, Wolczynska 133, 01–919, Warszawa, Poland*
[2]*Department of Physics, School of Engineering and Physical Sciences, Heriot-Watt University, Scottish Universities Physics Alliance, Edinburgh, EH14 4AS, UK*
[3]*Faculty of Physics, University of Warsaw, Pasteura 7, 02–093 Warszawa, Poland*
**rafal.kasztelanic@itme.edu.pl*

Abstract: We present a novel method for the development of a micro lenslets hexagonal array. We use gradient index (GRIN) micro lenses where the variation of the refraction index is achieved with a structure of nanorods made of 2 types of glasses. To develop the GRIN micro lens array, we used a modified stack-and-draw technology which was originally applied for the fabrication of photonic crystal fibers. This approach results in a completely flat element that is easy to integrate with other optical components and can be effectively used in high refractive index medium as liquids. As a proof-of-concept of the method we present a hexagonal array of 469 GRIN micro lenses with a diameter of 20 μm each and 100% fill factor. The GRIN lens array is further used to build a Shack-Hartmann detector for measuring wavefront distortion. A 50 lens/mm sampling density is achieved.

OCIS codes: (060.2280) Fiber design and fabrication; (060.4005) Microstructured fibers; (230.3990) Micro-optical devices; (110.2760) Gradient-index lenses; (010.7350) Wave-front sensing; (100.2550) Focal-plane-array image processors.

References and links

1. R. E. Troy, *Shack-Hartmann and Interferometric Hybrid Wavefront Sensor* (BiblioScholar, 2012).
2. M. Born and E. Wolf, *Principles of Optics*, 7thed. (Cambridge University Press, 1999).
3. M. Schwertner, M. J. Booth, and T. Wilson, "Wavefront sensing based on rotated lateral shearing interferometry," Opt. Commun. **281**(2), 210–216 (2008).
4. F. Roddier, M. Northcott, and J. E. Graves, "A simple low-order adaptive optics system for near-infrared applications," Publ. of Astr. Soc. of the Pacific **103**, 131–149 (1991).
5. R. Ragazzoni, E. Diolaiti, and E. Vernet, "A pyramid wavefront sensor with no dynamic modulation," Opt. Commun. **208**(1–3), 51–60 (2002).
6. R. Kasztelanic and A. Sagan, "Semiderivative real filter for microoptical elements quality control," Opt. Rev. **16**(3), 252–256 (2009).
7. R. Kasztelanic, "Amplitude filter and Zernike polynomial expansion method for quality control of microlens arrays," Appl. Opt. **49**(28), 5486–5492 (2010).
8. S. Welch, A. Greenaway, P. Doel, and G. Love, "Smart optics in astronomy and space," Astr. Geoph. **44**(1), 26–29 (2003).
9. P. Mercère, P. Zeitoun, M. Idir, S. Le Pape, D. Douillet, X. Levecq, G. Dovillaire, S. Bucourt, K. A. Goldberg, P. P. Naulleau, and S. Rekawa, "Hartmann wave-front measurement at 13.4 nm with lambdaEUV/120 accuracy," Opt. Lett. **28**(17), 1534–1536 (2003).
10. E. Li, Y. Dai, H. Wang, and Y. Zhang, "Application of eigenmode in the adaptive optics system based on a micromachined membrane deformable mirror," Appl. Opt. **45**(22), 5651–5656 (2006).
11. E. J. Fernandez, L. Vabre, B. Hermann, A. Unterhuber, B. Povazay, and W. Drexler, "Adaptive optics with a magnetic deformable mirror: Applications in the human eye," Opt. Express **14**(20), 8900–8917 (2006).
12. P. Godara, A. M. Dubis, A. Roorda, J. L. Duncan, and J. Carroll, "Adaptive optics retinal imaging: Emerging clinical applications," Optom. Vis. Sci. **87**(12), 930–941 (2010).
13. Spiricon, ed., *Hartmann Wavefront Analyzer Tutorial* (Spiricon, 2004).
14. D. R. Neal, J. Copland, and D. A. Neal, "Shack-Hartmann wavefront sensor precision and accuracy," Proc. SPIE **4779**, 148–160 (2002).

#277567 http://dx.doi.org/10.1364/OE.25.001680
Journal © 2017 Received 26 Sep 2016; revised 1 Jan 2017; accepted 6 Jan 2017; published 23 Jan 2017

Optics EXPRESS

15. M. Nicolle, T. Fusco, G. Rousset, and V. Michau, "Improvement of Shack-Hartmann wave-front sensor measurement for extreme adaptive optics," Opt. Lett. **29**(23), 2743–2745 (2004).
16. K. L. Baker and M. M. Moallem, "Iteratively weighted centroiding for Shack-Hartmann wave-front sensors," Opt. Express **15**(8), 5147–5159 (2007).
17. C. Leroux and C. Dainty, "Estimation of centroid positions with a matched-filter algorithm: relevance for aberrometry of the eye," Opt. Express **18**(2), 1197–1206 (2010).
18. J. Vargas, R. Restrepo, J. C. Estrada, C. O. Sorzano, Y. Z. Du, and J. M. Carazo, "Shack-Hartmann centroid detection using the spiral phase transform," Appl. Opt. **51**(30), 7362–7367 (2012).
19. W. H. Southwell, "Wavefront estimation from wavefront slope measurements," J. Opt. Soc. Am. **70**(8), 998–1006 (1980).
20. D. L. Fried, "Least-square fitting a wave-front distortion estimate to an array of phasedifference measurements," J. Opt. Soc. Am. **67**(3), 370–375 (1977).
21. C. R. Vogel, "Sparse matrix methods for wavefront reconstruction, revisited," Adv. in Adaptive Opt. **5490**, 1327–1335 (2004).
22. K. R. Freischlad and C. L. Koliopoulos, "Modal estimation of a wave front from difference measurements using the discrete Fourier transform," J. Opt. Soc. Am. A **3**(11), 1852–1861 (1986).
23. C. R. Vogel and Q. Yang, "Multigrid algorithm for least-squares wavefront reconstruction," Appl. Opt. **45**(4), 705–715 (2006).
24. P. J. Hampton, P. Agathoklis, and C. Bradley, "A New Wave-Front Reconstruction Method for Adaptive Optics Systems Using Wavelets," IEEE J. of Selected Topics in Sig. Proc. **2**, 781–792 (2008).
25. E. Thiébaut and M. Tallon, "Fast minimum variance wavefront reconstruction for extremely large telescopes," J. Opt. Soc. Am. A **27**(5), 1046–1059 (2010).
26. M. Rosensteiner, "Cumulative Reconstructor: fast wavefront reconstruction algorithm for Extremely Large Telescopes," J. Opt. Soc. Am. A **28**(10), 2132–2138 (2011).
27. C. C. de Visser and M. Verhaegen, "Wavefront reconstruction in adaptive optics systems using nonlinear multivariate splines," J. Opt. Soc. Am. A **30**(1), 82–95 (2013).
28. A. Polo, V. Kutchoukov, F. Bociort, S. F. Pereira, and H. P. Urbach, "Determination of wavefront structure for a Hartmann Wavefront Sensor using a phase-retrieval method," Opt. Express **20**(7), 7822–7832 (2012).
29. J. Vargas, R. Restrepo, and T. Belenguer, "Shack-Hartmann spot dislocation map determination using an optical flow method," Opt. Express **22**(2), 1319–1329 (2014).
30. R. Fontaine, "The state-of-the-art of mainstream CMOS image sensors," in Proceedings IEEE Xplore Conference: 37th European Solid State Device Research Conference, ESSDERC (IEEE 2007).
31. C. Gómez-Reino, M. V. Perez, and C. Bao, *Gradient-index Optics: Fundamentals and Applications* (Springer, Berlin, 2002).
32. C. Gómez-Reino, M. V. Perez, C. Bao, and M. T. Flores-Arias, "Design of GRIN optical components for coupling and interconnects," Laser Photonics Rev. **2**(3), 203–215 (2008).
33. R. W. Gilsdorf and J. C. Palais, "Single-mode fiber coupling efficiency with graded-index rod lenses," Appl. Opt. **33**(16), 3440–3445 (1994).
34. A. G. Mignani, A. Mencaglia, M. Brenci, and A. Scheggi, "Radially Gradient-Index Lenses: Applications to Fiber Optic Sensors," in *Diffractive Optics and Optical Microsystems*, S. Martellucci, A. N. Chester ed. (Springer US, 311–325, 1997).
35. L. Fu, X. Gan, and M. Gu, "Characterization of gradient-index lens-fiber spacing toward applications in two-photon fluorescence endoscopy," Appl. Opt. **44**(34), 7270–7274 (2005).
36. J. R. Hensler, "Method of Producing a Refractive Index Gradient in Glass," U.S. Patent 3,873,408 (25 Mar. 1975).
37. J. Teichman, J. Holzer, B. Balko, B. Fisher, and L. Buckley, "Gradient Index Optics at DARPA," Institute For Defense Analyses Alexandria Va (2013).
38. GRINTECH GmbH website: www.grintech.de.
39. Y. Huang and S. T. Ho, "Superhigh numerical aperture (NA > 1.5) micro gradient-index lens based on a dual-material approach," Opt. Lett. **30**(11), 1291–1293 (2005).
40. F. Hudelist, R. Buczynski, A. J. Waddie, and M. R. Taghizadeh, "Design and fabrication of nano-structured gradient index microlenses," Opt. Express **17**(5), 3255–3263 (2009).
41. T. Martynkien, D. Pysz, R. Stępień, and R. Buczyński, "All-solid microstructured fiber with flat normal chromatic dispersion," Opt. Lett. **39**(8), 2342–2345 (2014).
42. R. Buczyński, M. Klimczak, T. Stefaniuk, R. Kasztelanic, B. Siwicki, G. Stępniewski, J. Cimek, D. Pysz, and R. Stępień, "Optical fibers with gradient index nanostructured core," Opt. Express **23**(20), 25588–25596 (2015).
43. F. Hudelist, J. M. Nowosielski, R. Buczynski, A. J. Waddie, and M. R. Taghizadeh, "Nanostructured elliptical gradient-index microlenses," Opt. Lett. **35**(2), 130–132 (2010).
44. J. M. Nowosielski, R. Buczynski, F. Hudelist, A. J. Waddie, and M. R. Taghizadeh, "Nanostructured GRIN microlenses for Gaussian beam focusing," Opt. Commun. **283**(9), 1938–1944 (2010).
45. J. Nowosielski, R. Buczynski, A. J. Waddie, A. Filipkowski, D. Pysz, A. McCarthy, R. Stepien, and M. R. Taghizadeh, "Large diameter nanostructured gradient index lens," Opt. Express **20**(11), 11767–11777 (2012).
46. A. Filipkowski, B. Piechal, D. Pysz, R. Stepien, A. Waddie, M. R. Taghizadeh, and R. Buczynski, "Nanostructured gradient index microaxicons made by a modified stack and draw method," Opt. Lett. **40**(22), 5200–5203 (2015).

Optics EXPRESS

47. J. Pniewski, R. Kasztelanic, J. M. Nowosielski, A. Filipkowski, B. Piechal, A. J. Waddie, D. Pysz, I. Kujawa, R. Stepien, M. R. Taghizadeh, and R. Buczynski, "Diffractive optics development using a modified stack-and-draw technique," Appl. Opt. **55**(18), 4939–4945 (2016).
48. A. J. Waddie, R. Buczynski, F. Hudelist, J. M. Nowosielski, D. Pysz, R. Stepien, and M. R. Taghizadeh, "Form birefringence in nanostructured micro-optical devices," Opt. Mater. Express **1**(7), 1251–1261 (2011).
49. R. Buczynski, I. Kujawa, R. Kasztelanic, D. Pysz, K. Borzycki, F. Berghmans, H. Thienpont, and R. Stepien, "Supercontinuum generation in all-solid photonic crystal fiber with low index core," Laser Phys. **22**(4), 784–790 (2012).
50. J. Pniewski, T. Stefaniuk, G. Stepniewski, D. Pysz, T. Martynkien, R. Stepien, and R. Buczynski, "Limits in development of photonic crystal fibers with a subwavelength inclusion in the core," Opt. Mater. Express **5**(10), 2366–2376 (2015).
51. M. Harker and P. J. O'Leary, "Regularized Reconstruction of a Surface from its Measured Gradient Field," J. Math. Imaging Vis. **51**(1), 46–70 (2015).

1. Introduction

The Shack-Hartmann (S-H) sensor [1] is a device commonly used for measuring wavefront distortion. Other devices or methods allowing for the similar measurements are: phase-shift [2] and shearing [3] interferometry methods, laser ray tracing, curvature sensor [4], pyramid wavefront sensor [5], spatially resolved refractometry and methods based on such spatial filters as the semiderivative filter [6, 7]. The wavefront distortion, i.e. phase changes of the propagating electromagnetic wave, can be caused by the distortion of the medium (e.g. atmosphere or tissue) where the light wave is propagating, or by the shape of the element that the wave penetrates or is reflected by. That is why the measurement of the wevefront distortion, as well as visualization and measurement of phase objects is an important element of various contemporary domains of science, industry and medicine.

The S-H detector is most widely applied in a technology called adaptive optics, which involves measuring, reconstructing and reshaping the phase of a wavefront in real-time. The technology is used for example in astronomy [8], lithography [9], free space optical communication, telecommunication (for coupling eigenmode) [10], and in medicine [11, 12]. The idea underlying the S-H sensor is the observation that the local wavefront distortion φ in a point (x,y) may be determined based on analyzing the shift of the spot of a focused beam (Fig. 1(a)). Currently reported S-H sensors are based on refractive microlens arrays. They offer a sampling density in the range from 1 to 10 lens/mm when the minimum diameter of the lens is 100 μm. Smaller lenses are not used due to technological limitation. Lenses below 100 μm in diameter whose curvature is accurate are difficult to obtain. Moreover, the performance of refractive lensed is limited to air. For liquids, where the refractive index exceeds 1.33, their performance is degraded.

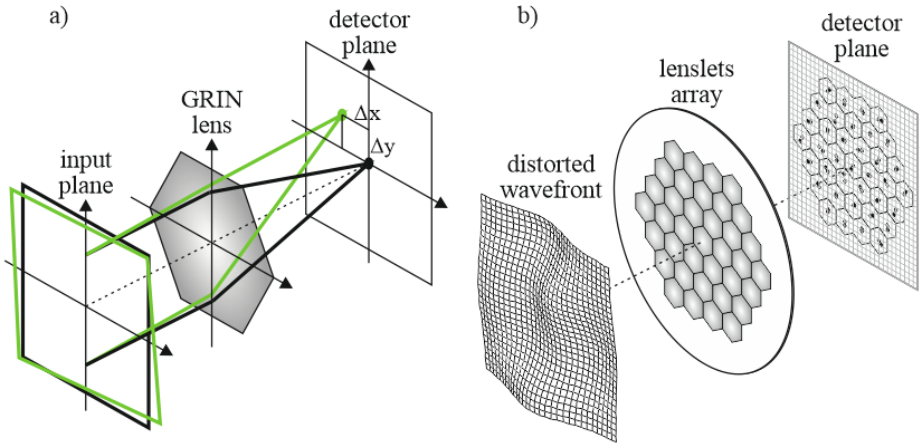

Fig. 1. Scheme of the Shack-Hartmann setup: a) determining the shift of the spot for a single GRIN lens, b) a full Shack-Hartmann setup.

Optics EXPRESS

To determine the wavefront distortion, the input wavefront is divided into smaller sub-regions with the use of a microlense array. A high resolution detector e.g. CCD camera is placed at the focal length behind the array. At the calibration stage, the setup is lit by the plane wave. Each lenslet (l) focuses a part of the incoming wavefront to a spot on the CCD. As a result, the referential location (x_{l0}, y_{l0}) of the center of each lenslet is obtained. Now, if the incoming wavefront is distorted, the light at a single lenslet will deflect. If the wavefront distortion is not too large, it is possible to determine where the focus of each lenslet (x_l, y_l) has shifted. This displacement is measured and used to find the local tilt of the wavefront based on the equation [13]:

$$\Delta x_l = x_{l0} - x_l = \kappa_x \frac{\partial \varphi(x_l, y_l)}{\partial x}$$
$$\Delta y_l = y_{l0} - y_l = \kappa_y \frac{\partial \varphi(x_l, y_l)}{\partial y} \quad (1)$$

where κ_x, κ_y are constant parameters determined by the geometry of a given optical setup in x and y direction, respectively.

If the wavefront is too curved, the spots will become blurred due to defocus, which makes it difficult to determine the center of the spot. The spot can also shift to such an extent that it is located in the focal spot of another lens. Because the distortions and shifts differ, there are various methods of determining the center of all the lens spots. The most important algorithms used here are: center of mass [14], weighted center of gravity [15], the iteratively weighted centroiding [16], matched filter approaches [17], and spiral phase transform [18]. Knowing many local Δx and Δy values, we can estimate the phase aberration with the use of a number of algorithms, such as: the zonal reconstruction method [19, 20], phase-retrieval or modal reconstruction method [21], methods based on the fast Fourier transform [22], multigrid [23], wavelet-based [24], fractal iterative [25], cumulative reconstructor [26], spline-based [27], non-linear intensity phase retrieval [28] and methods based on optical flow [29]. For a better reconstruction of the wavefront distortion, some of these methods additionally apply light distribution on the spots.

When designing a S-H sensor light economy is an issue. Due to a large number of lenslets the input light intensity is divided into small portions focused on the camera. The detection of such noisy signal is hard, so it is important that the lenslet array should absorb as little light as possible and that the fill factor should be close to 100%.

In this paper we present a setup for wavefront measurement based on a S-H sensor, whose main element is a thin hexagonal array of flat GRIN microlenses with 100% fill factor. The array composed of 469 micro-lenses with 20 μm diameter of single lens and high numerical aperture NA = 0.5. This provides high sampling density, with can be used with modern CCD or CMOS cameras, where the single pixel size is ~1 μm [30]. Moreover, the performance of the proposed flat GRIN microlenses array is not limited only to air but it can also be used to measurement e.g. in aqueous. We also present a novel approach to the fabrication such a hexagonal array of GRIN micro lenslets based on nanostructured approach, as well as the optical properties of the fabricated structure.

2. GRIN lenses

Refractive lenslets are used as a standard in microlens arrays in the S-H sensors. Here, we propose to use flat, gradient index elements as lenses because of their high numerical apertures (NA = 0.5, relative to NA = 0.015 in conventional detectors), high fill factor up to 100% and high light efficiency due to the small thickness (tens of microns). Gradient index (GRIN) components are micro-optical elements made from inhomogeneous medium in which the refractive index varies from point to point [31]. An example of such an element is a planar-surface GRIN lens. The planar nature of GRIN elements makes them attractive for

Optics EXPRESS

compact optical systems, since they can be easily integrated with fibers, detectors, sources and other micro-optical components [32]. In particular, they have been used to construct micro-optic devices such as optical couplers, connectors, beam splitters, optical attenuators, beam expanders, optical fiber switches [32, 33] and applied in in optical sensing [34] and endoscopy [35].

There are several standard methods of GRIN microlens fabrication. A widely used technique is the ion exchange process [36]. Other techniques include [37]: neutron irradiation, chemical vapor deposition (CVD), polymerization, ion stuffing, crystal growing, sol-gel, droplet on demand and multi-layer coextrusion. However, each of these methods is not flawless, the most important flaws including very small contrasts, the inaccuracy of the refractive index distribution, and the possibility of only monotonic refractive index distributions. The standard difference of the refraction indexes Δn is 0.1 at the length of 250 μm [38]. Obtaining larger gradients, e.g. $\Delta n = 0.25$ per 6.5 μm [39], has been demonstrated in 1D multilayer GRIN, fabricated with the use of chemical vapor deposition.

Recently, we have introduced a method which allows for producing 2D gradient index lenses with internal nanostructures and a very high gradient of refractive index [40]. The method allows for fabricating arbitrary index distributions within the limits of the refractive index constants of about $\Delta n \approx 0.3$ and a maximum gradient of about $\Delta n \approx 0.3$ per 1 μm. Using the method, we have made such optical elements as: an all-solid microstructured fiber [41, 42], elliptical gradient lens [43], lens for Gaussian beam focusing [44] large diameter GRIN lens [45], axicon [46], DOE [47] and birefrigement [48] elements.

3. Description of the GRIN Shack-Hartmann sensor development method

To develop the array of GRIN microlenslets we have used the stack-and-draw process. The technique consists of several steps shown in Fig. 2.

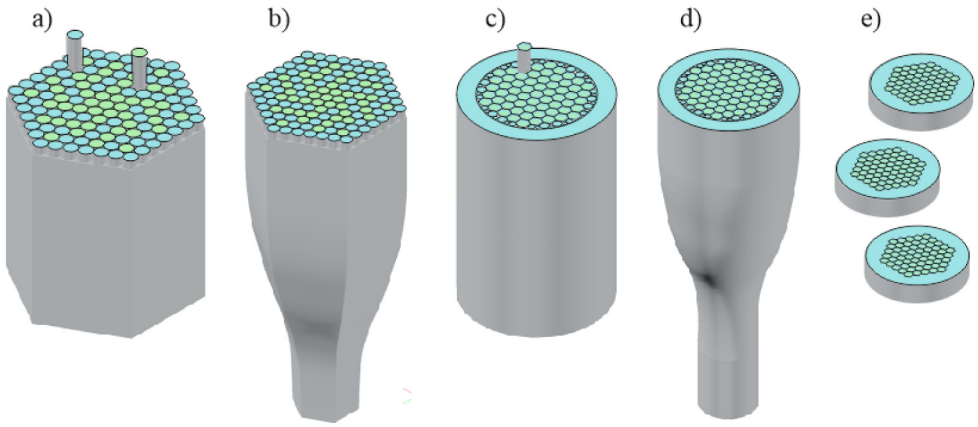

Fig. 2. Schematic of the modified stack-and-draw technique: a) preform stacked with two kinds of glass, b) drawing hexagonal preform, c) stack array of GRIN lenlets, d) drawing the final structure, e) cut and polished array of GRIN lenslets.

First, we prepare round rods, approximately 0.5 mm in diameter, made from two types of glasses. One is an in-house synthesized low-index silicate glass NC21 (55% SiO2, 1% Al2O3, 26% B2O3, 3% Li2O, 9.5% Na2O, 5.5% K2O, 0.8% As2O3) and the second a commercially available high-index lead-silicate glass F2. The refraction index characteristics for both glasses and the refraction index difference Δn are shown in Fig. 3. Both glasses are thermally matched and have been successfully used previously [47, 49].

Optics EXPRESS

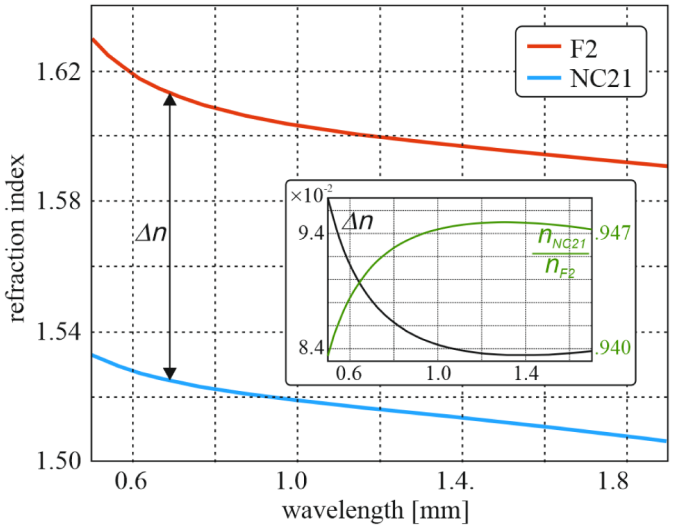

Fig. 3. The refractive index, the refractive index difference Δn and the ratio of n_{NC21}/n_{F2} as a function of the wavelength for the NC21 and F2 glasses.

Next, the rods from both glasses are stacked to hexagonal preform according to the desired pattern (Fig. 2(a)). In our case the preform consist of 7651 rods and the pattern chosen such that the average refractive index corresponds to parabolic refractive index distribution in GRIN lens (Fig. 4):

$$n = n_{F2}\left(1 - \frac{A}{2}r^2\right) \tag{2}$$

where: n_{F2} is a refractive index of F2 glass, r changes from 0 in the center of the lens to 1 at its outer edge and constant $A = 0.1052$ is chosen such that the refraction index n equals the refraction index of NC21 glass for $r = 1$ and the wavelength $\lambda = 1\mu m$:

$$A = 2\frac{\Delta n}{n_{F2}} = 2 - \frac{n_{NC21}}{n_{F2}} \tag{3}$$

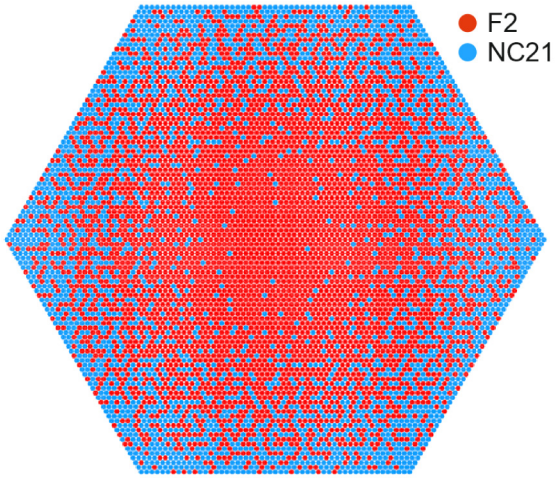

Fig. 4. Design of a preform for a GRIN lens composed of 7651 rods made from two glasses.

Optics EXPRESS

As the following step, the hexagonal preform (Fig. 2(b)) is drawn, which scales it down approximately 25 times. The result of this process is a hexagonal GRIN lens, approximately 1 mm in diameter. Next, the element obtained is cut into segments of 10 cm and another preform of 469 such rods is stacked and embedded into an NC21 tube. The free space between the tube and the hexagonal lens structure is filled with additional NC21 rods (Fig. 2(c)). The next step consists in drawing the final structure to fiber with the diameter of 318.5 µm (Fig. 2(d)). In the last step the fiber structures are cut into slices, grounded and polished to the required thickness, which is typically 50 µm to 100 µm (Fig. 2(e)). It is essential that the fabricated elements have the same thickness of their entire surface.

Using the stack-and-draw process we can fabricate a hexagonal array of GRIN microlenses, where the diameter of a single lens is 20 µm, and the fill factor is 100% (Fig. 5). Each lens has the same optical properties, with high precision. The size-limiting factor is the diffusion process between glasses [50]. This limits the size of the single rod to ~100 nm, and the diameter of a single lens to ~10 µm.

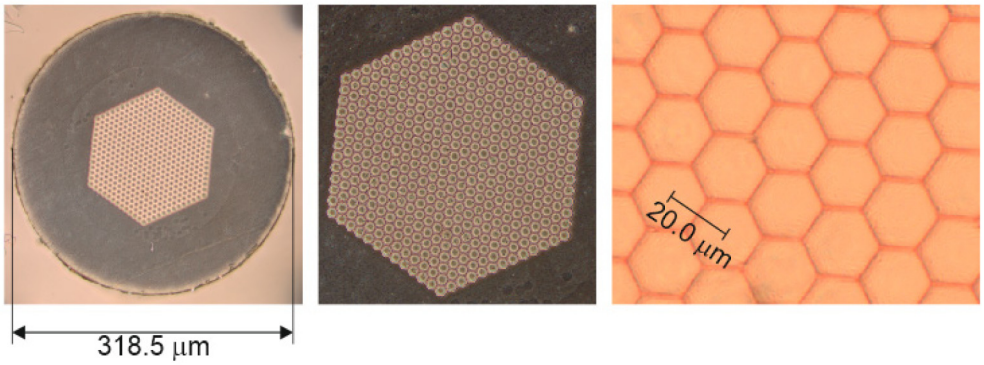

Fig. 5. Array of micro GRIN lenslets fabricated by using stack-and-draw technique.

4. Experimental verification of a Shack-Hartman sensor

At the first stage of checking the quality of the fabricated elements, we tested the imaging (Fig. 6(a)) and focusing capabilities of the elements of varied thickness (Fig. 6(b)). A crucial characteristic of the fabricated element of a given thickness is also the focus of a single lens, which depends only on the ratio or difference in the refractive index of both glasses (Eq. (3), in accordance with the equation (equation for SELFOC lens [50]):

$$f = \frac{1}{n_{F2}\sqrt{A}\sin\left(t\sqrt{A}\right)} \tag{4}$$

where t is a lens thickness. As shown in Fig. 3, the difference Δn changes only slightly for a wide range of wavelengths, due to which the focus length also changes only to a small extent. For the tested element, with thickness of 75 µm the measured focal length (from end of lens to focus plane) is 50 µm for the wavelength range from 0.5 to 1.5 µm. As measured, the acceptance angle is 14° and quarter-pitch is about 135 µm.

Optics EXPRESS

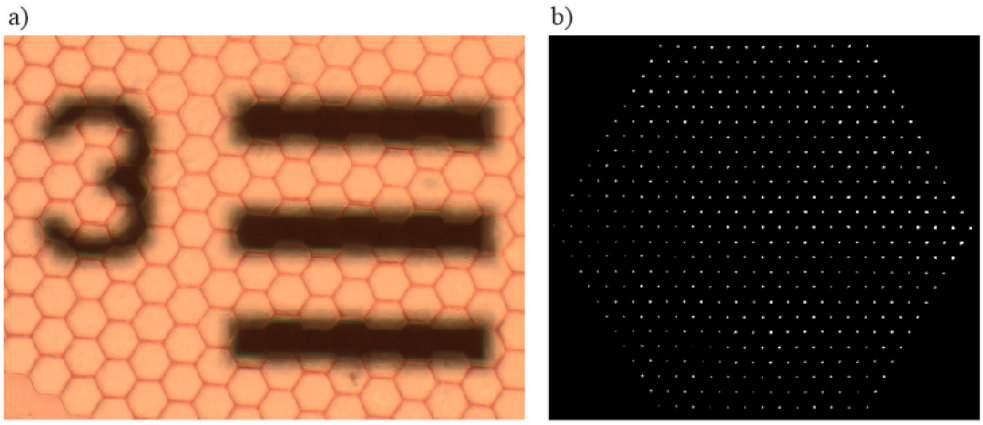

Fig. 6. GRIN lenslet array: a) imaging of the test object with a resolution 20.16 pl/mm (3rd element of 4th group in the 1951 USAF Resolution Test Targets), b) light intensity on focal plane for a non-distorted wavefront.

The S-H detector was built in two configurations (Fig. 7). In the first case, we tried to build a setup of minimal size, where the fabricated array of GRIN lenslets was straight on the CCD camera detector (Fig. 7(a)). However, due to the detector's protective glass of 1.2 mm and due to problems with preserving the submicron precision when cutting and polishing the lenslets array, we did not manage to obtain good enough quality of focusing on the CCD detector. The numerical analysis shows that in order to focus light exactly on the CCD plane, as described above, the thickness of the microlens array should equal 7.56 μm. Optical elements of this thickness, however, are very difficult to handle. Moreover, the thickness change of 10 nm changes the location of the focus by nearly 1.5 μm, which places very high demands on the entire process of cutting and grinding of the sample. Focusing light on the CCD plane is also possible for a sample thickness of 279 μm, which eliminates some of the problems. But here the accuracy of cutting and grinding is also required in the order of 10 nm. One of the possible methods to reduce these problems is to use two glasses with a smaller refractive index difference. The optimal solution to the above-mentioned problem is replacing the cover glass of the CCD detector by our flat element whose thickness equals a quarter-pitch, which is 135 μm. This would ensure the compact size of the detector, but unfortunately the technological limitations did not allow us to build such a setup.

In the second setup, the focal plane for the GRIN lenslets array was imaged on the CCD with the use of a microscope objective magnifying x40 (Fig. 7(b)). In this approach, the S-H detector can be set for an array of GRIN lenslets of varied thickness and for various detectors. Furthermore, for this setup the requirements for precision cutting and polishing are orders of magnitude smaller than for a compact setup. In this case, changing the thickness by 1 μm changes the location of the focus by less than 1 μm. Additionally, the setup allows to scale the image displayed on the detector, which allows to choose the scale, e.g. depending on the size of a single pixel of the camera. The use of the additional optical elements like microscope objectives give the possibility of introducing systematic aberrations. However, they can be considered and eliminated at the stage of numerical wavefront distortion reconstruction.

Optics EXPRESS

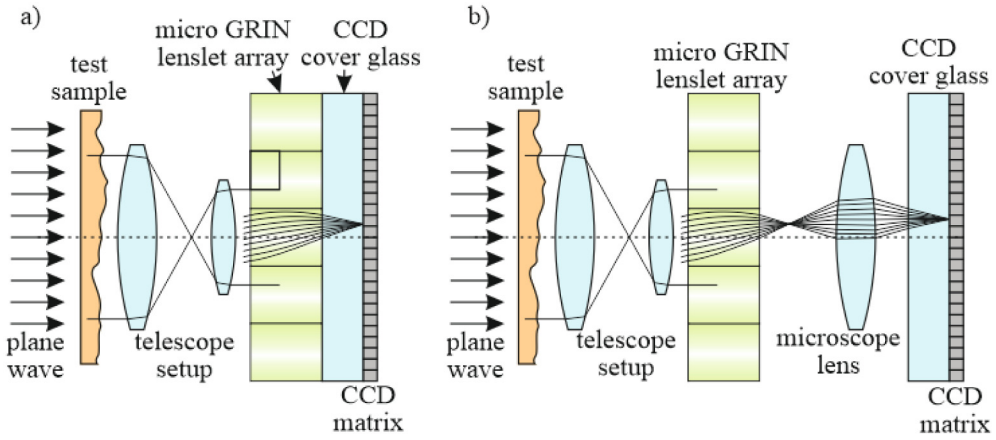

Fig. 7. Scheme of the Shack-Hartmann sensor setup: a) compact setup, b) setup witch microscope objective.

As test objects introducing wavefront distortion of known parameters, we used a refractive lens with focal length $f = 25$ mm, and an array of refractive lenslets (MLA150-5C Thorlabs) with focal length $f = 5.2$ mm, diameter $d = 146$ µm and pitch $p = 150$ µm.

In each case, we first registered the reference image without the tested element, and then with the tested element placed in the setup, we registered the image with shifted foci. Because the area of maximum search for each lens is hexagonal (Fig. 8(a)) and there is no time limit for the search, the location of each spot can be determined by adjusting a 2D Gaussian distribution to the intensity distribution after rejecting the pixels of intensity lower than 25% of the maximum (Fig. 8(b)).

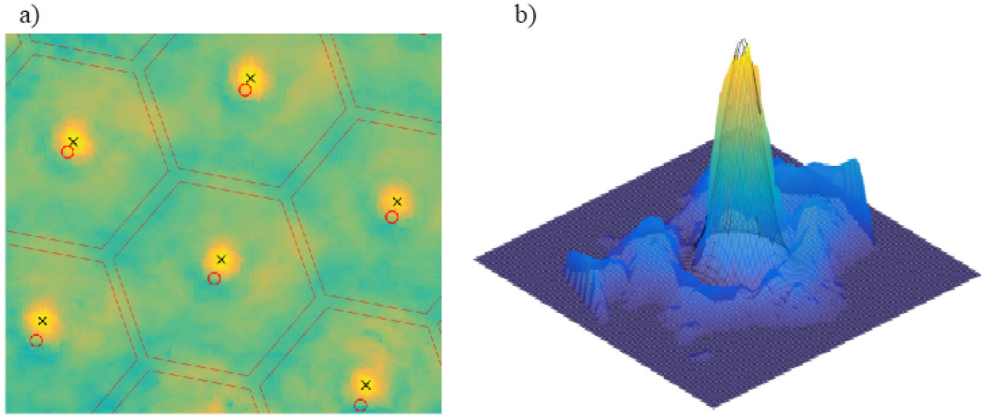

Fig. 8. Scheme of finding the center spot for one lens: a) search area (red circle – geometrical center, black cross – found spot center), b) adjusting 2D Gaussian distribution.

The shifts in 469 points calculated based on Eq. (1) allowed us to establish the wavefront distortion with the use of regularized reconstruction method [51]. The results for a single refractive lens together with a map of reconstruction errors are presented in Fig. 9. The absolute reconstruction error:

$$\Delta\varphi = \varphi_0 - \varphi_m \tag{5}$$

Optics EXPRESS

was equal 0.2 deg, where φ_0 and φ_m are the original shape (curvature) and the measured shape (curvature), respectively. The relative reconstruction error calculated as $\Delta\varphi / \varphi_0$ was at the level of 3%.

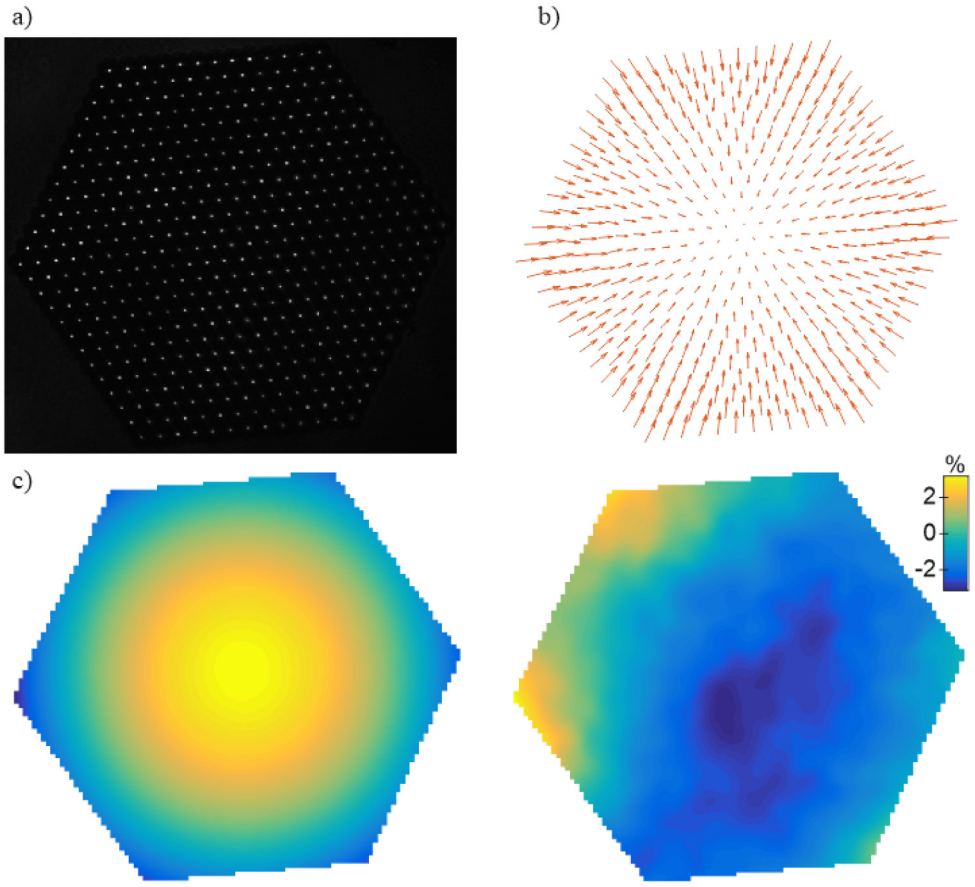

Fig. 9. Results of testing wavefront distortion for single refractive lens: a) light intensity of distorted wavefront on CCD plane, b) map of shifts in 469 points, c) reconstructed shape of the wavefront distortion, d) map of relative reconstruction error.

The results of measurements of the wavefront distortion for an array of refractive lenslets are presented in Fig. 10. From Fig. 10(a) we can see that the wavefront distortion introduced by a single lenslet of diameter 150 μm was 'analyzed' by ~40 GRIN microlenslets. Reconstructing the shape (curvature) of the examined element is possible, but the relative reconstruction errors are larger and equal ~23%, with a similar absolute errors (equaling 0.19 deg) as in the measurement of the first element.

The results obtained are hard to compare to the existing setups because setups of such high resolution do not exist. It is worth mentioning that the second element examined – the microlenslet array – is a standard element utilized in commercially available S-H setups.

Optics EXPRESS

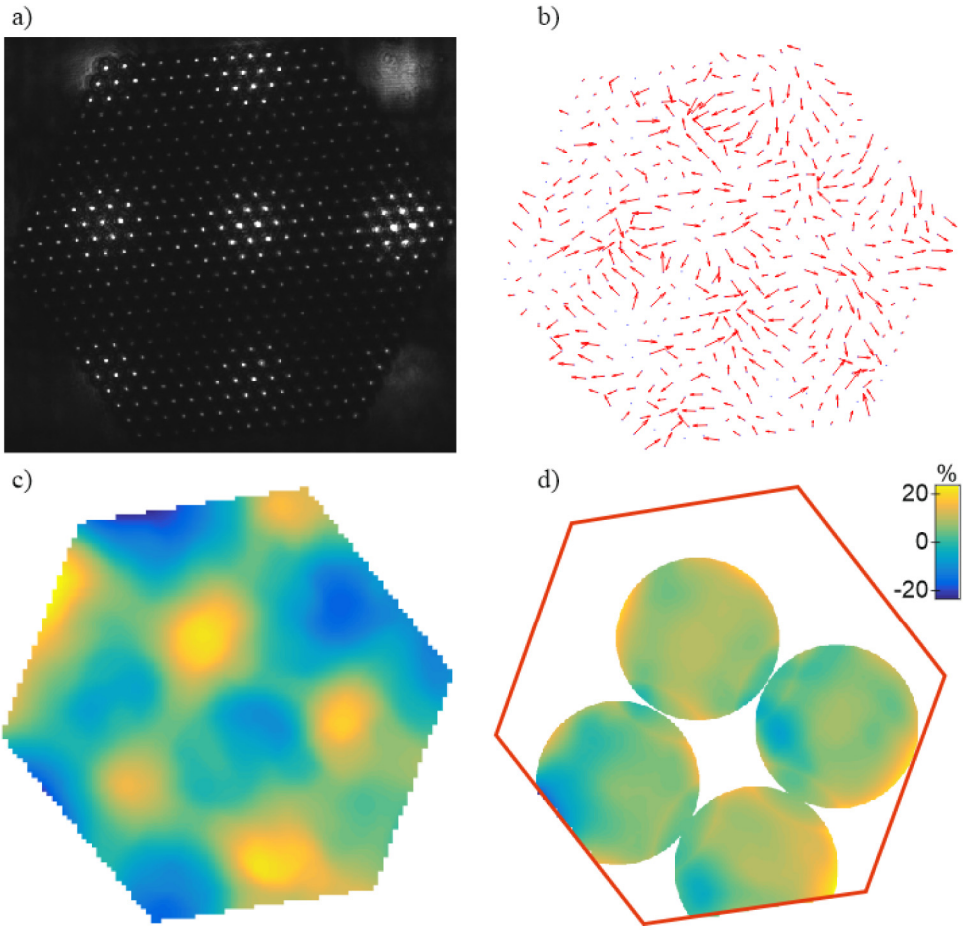

Fig. 10. Measurement results of wavefront distortion for an array of refractive microlenses: a) comparison of the scale of the measured element with a GRIN lenslet array, b) light intensity of distorted wavefront on CCD plane, c) map of shifts in 469 points, d) reconstructed shape of the wavefront distortion, e) map of relative reconstruction error for four central microlenses.

5. Conclusions

We have demonstrated that it is possible to develop a flat array of micro GRIN lenslets using the modified stack-and-draw technique. In the paper, we have presented an array composed of 469 micro-lenses (20 µm diameter of single lens) arranged in a hexagonal structure of 100% fill factor. We have verified that the fabricated element can be used as a part of the Shack-Hartman detector, and that such a detector can be applied to examine the wavefront, or to examine the shape of elements with a very high sampling density (50 lens/mm), although earlier S-H sensors often did not offer sampling density better than 10 lens/mm. Such a high sampling density can be used with modern CCD or CMOS cameras, where the single pixel size is ~1 µm. High-sampling density, similar to the resolution of the GRIN lenslets array, can be used to study wavefront distortion with a high resolution, for example in microfluidics setups or in biology for imaging plankton. Low thickness (below 100 µm), short focus length, 100% fill factor and flatness make the array highly light-efficient. Since GRIN array has a flat facade, the optical performance of lenses is not degraded, even if the array is immersed in medium other than air. This opens a unique opportunity to measure the phase front of the light beam propagating in liquids, not restricted to water but also including such high-index media as organic liquids.

Optics EXPRESS

Our method offers the possibility to fabricate an array composed of smaller lenslets (~10 μm in diameter), an array where the lenses are not arranged hexagonally, and an array composed of other optical elements of an arbitrary refractive index distribution.

Funding

National Science Centre in Poland (HARMONIA UMO-2013/10/M/ST3/00708 and TANGO TANGO1/269956/NCBR/2015).